AN APPLICATION OF SMALL-GAP EQUATIONS IN SEALING DEVICES

Carlos A. Vionnet and Juan C. Heinrich
Department of Aerospace and Mechanical Engineering
University of Arizona
Tucson, Arizona 85721

SUMMARY

The study of a thin, incompressible Newtonian fluid layer trapped between two almost parallel, sliding surfaces has been actively pursued in the last decades. This subject includes lubrication applications such as slider bearings or the sealing of non-pressurized fluids with rubber rotary shaft seals. In the present work we analyze numerically the flow of lubricant fluid through a micro-gap of sealing devices. The first stage of this study is carried out assuming that a 'small-gap' parameter δ attains an extreme value in the Navier-Stokes equations. The precise meaning of small-gap is achieved by the particular limit $\delta = 0$ which, within the bounds of the hypotheses, predicts transport of lubricant through the sealed area by centrifugal instabilities. Numerical results obtained with the penalty function approximation in the finite element method are presented. In particular, the influence of inflow and outflow boundary conditions, and their impact in the simulated flow are discussed.

INTRODUCTION

Most seals are relatively simple elements widely employed in diverse types of rotary machines. This sealing component is often used to seal rotating shafts at low oil pressures, avoiding the transport of contaminant to, or lubricant from, the equipment it protects. The seal, bonded to the oil reservoir, is stationary and presents a narrow section that slides over the moving surface of the rotary shaft. Fig.1 shows a cross section of the geometry under consideration.

The device is designed to have an interference with the shaft. Therefore, once the piece is mounted, the compliance of the elastic body ensures a perfect fit between the seal and the cylindrical surface of the shaft. Under these conditions, some of the initial asperities of the seal wear out after a brief period of time, leaving an extremely thin layer of lubricant fluid that separates the surfaces in contact. This was first noticed by Jagger (ref.1) and, ever since, numerous explanations attempted to account for two consequences of this experimental fact: the hydrodynamic force able to sustain a gap between the two bodies and the mechanisms that prevent the fluid from leaking through. Jagger proposed that the surface tension of the sealed fluid controls leakage thanks to a meniscus formed on the air side. Kawahara and Hirabayashi (ref.2) observed that a properly installed and functional seal leaked when the installation is reversed.

With the assumption of relative parallel sliding between two rough surfaces, lubrication theory has been the chosen tool by many researchers to answer these fundamental problems (see e.g. ref.3). The load-carrying capacity of parallel sliding of rough surfaces was first studied by Davies (ref.4). Later on, Jagger and Walker (ref.5) assumed that the asperities act as micro-bearings pads in the contact area. However, Lebeck (refs.6 and 7) concluded that none of the existing models can fully explain the sliding motion as commonly observed in experiments. Gabelli and Poll (ref.8) studied the dominant action of the surface microgeometry in the formation of the lubricant

film. They found that the contribution of mechanical pressure to the load-carrying capacity due to body contact is very small and indeed negligible. Salant (ref.9) claimed that micro-undulations in the lip surface restrict leakage by virtue of a 'reverse-pumping' process in which fluid is driven from the low to the high pressure side. However, no one has really observed such micro-undulations, either in static or dynamic conditions (ref.10).

Combinations of angular velocity and system eccentricity beyond the ability of the sealing device to maintain contact with the shaft would cause the seal to leak profusely. It has been suggested that an inherent pumping mechanism (ref.11), sufficient to counterbalance those influences promoting leakage, would be given by a relative motion between the sealing surfaces. Besides all these explanations, at present there is a wide gap between theory and practice, and a feasible explanation of the mechanism involved in the sealing action is still pending, even though elastomeric seals have been used extensively since the 1940's.

In the next section, we establish the small-gap equations using a rather simple order-of-magnitude analysis. This is followed by numerical examples showing the validity of the proposed model and the influence of the boundary conditions in the numerical predictions.
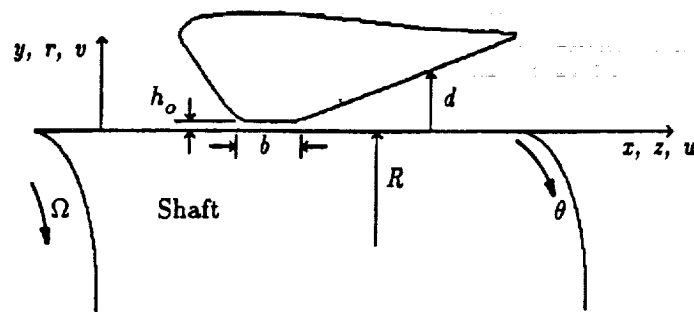

fig. 1 - Cross section of a typical sealing device

ANALYTICAL MODEL

We assume an oil-film already formed ignoring any mechanical contact between the sealing device and the shaft, as well as any distortion of the upper elastic seal. We consider a thin viscous liquid layer bounded above by a smooth surface and below by a perfectly rounded shaft, without including edge effects such as the meniscus experimentally observed on the air-side (ref.1). Despite the fact that the film within the gap is very thin, we assume it to be thick enough to conform to the continuum hypothesis. There is no local rupture of the film such as cavitation or dry spots in the contact area, and the layer consists of an incompressible Newtonian fluid with constant properties under isothermal conditions.

We begin with the Navier-Stokes equations written in cylindrical coordinates (ref.12), setting the direction of the line $r = 0$ coincident with the shaft axis

$$\frac{1}{r}\frac{\partial(ru_r)}{\partial r} + \frac{1}{r}\frac{\partial u_\theta}{\partial \theta} + \frac{\partial u_z}{\partial z} = 0 \tag{1}$$

$$\frac{\partial u_r}{\partial t} + \vec{u}.grad(u_r) - \frac{u_\theta^2}{r} = -\frac{1}{\rho}\frac{\partial p}{\partial r} + \nu\left(\Delta u_r - \frac{2}{r^2}\frac{\partial u_\theta}{\partial \theta} - \frac{u_r}{r^2}\right) \tag{2}$$

500

$$\frac{\partial u_\theta}{\partial t} + \vec{u}.grad(u_\theta) + \frac{u_r u_\theta}{r} = -\frac{1}{\rho r}\frac{\partial p}{\partial \theta} + \nu\left(\Delta u_\theta + \frac{2}{r^2}\frac{\partial u_\theta}{\partial \theta} - \frac{u_\theta}{r^2}\right) \tag{3}$$

$$\frac{\partial u_z}{\partial t} + \vec{u}.grad(u_z) = -\frac{1}{\rho}\frac{\partial p}{\partial z} + \nu\,\Delta u_z \tag{4}$$

where

$$\vec{u} = (u_r, u_\theta, u_z) \quad , \quad grad = \left(\frac{\partial}{\partial r}, \frac{1}{r}\frac{\partial}{\partial \theta}, \frac{\partial}{\partial z}\right) \quad , \quad \Delta = \frac{1}{r}\frac{\partial}{\partial r}\left(r\frac{\partial}{\partial r}\right) + \frac{1}{r^2}\frac{\partial^2}{\partial \theta^2} + \frac{\partial^2}{\partial z^2}$$

In absence of a free surface the gravitational body force is expressed as the gradient of a scalar quantity and, therefore, it has been included in the pressure gradient term.

The analysis of the lubricant flow in the micro-gap involves, roughly speaking, three disparate length scales, namely, the radius R of the shaft ($\sim 0.04m$), the much smaller thickness h_o of the fluid ($\sim 10\mu m$) and an intermediate length b characterizing the axial extent of the contact region ($\sim 200\mu m$) (see fig. 1). Next, the Navier-Stokes equations, once recast with the aforementioned scales, are simplified by letting the ratio between the gap height and the radius of the shaft formally approach zero.

Inner region: lubrication regime

Given the tiny thickness of the lubricant film, radial oscillations proportional to the gap height will alter considerably the flow inside the micro-gap. To analyze this effect, consider a shaft rotating at angular velocity Ω and separated an average distance h_o from the stationary seal (fig.1). Introducing now

$$(x,y,\xi) \rightarrow \left(\frac{z}{h_o}, \frac{r-R}{h_o}, \theta\right) \qquad , \qquad \tau \rightarrow \Omega t \tag{5}$$

$$(u,v,w) \rightarrow \left(\frac{u_z}{\Omega h_o}, \frac{u_r}{\Omega h_o}, \frac{u_\theta}{\Omega R}\right) \quad , \quad p^* \rightarrow \frac{(p-p_a)}{\rho\nu\Omega} \tag{6}$$

into the equations of motion (1)-(4), and letting $\delta = \frac{h_o}{R}$ formally approach zero while holding everything else fixed, we get

$$\nabla.\vec{u} = 0 \tag{7}$$

$$\sigma\left(\partial_\tau + \vec{u}.\nabla\right)\vec{u} - R_e\,w^2\,\hat{j} = -\nabla p^* + \nabla^2\vec{u} \tag{8}$$

$$\sigma\left(\partial_\tau + \vec{u}.\nabla\right)w = \nabla^2 w \tag{9}$$

where

$$\vec{u} = (u,v) \quad , \quad \nabla = \left(\frac{\partial}{\partial x}, \frac{\partial}{\partial y}\right) \quad , \quad \hat{j} = (0,1)$$

and

$$R_e = \frac{\Omega R h_o}{\nu} \qquad : \text{Reynolds number} \tag{10}$$

$$\sigma = \frac{\Omega h_o^2}{\nu} \qquad : \text{squeezing Reynolds number} \tag{11}$$

Several other scaling are possible (ref.13), but this particular choice seems to be consistent with Gabelli and Poll observations (ref.8). They stated that the average

pressure gradient in the circumferential direction is indeed negligible when compared with the pressure gradient across the sealing contact. The squeezing Reynolds number σ is commonly so small that inertia terms can be neglected and the classical lubrication theory can be applied. Moreover, for small R_e, as it turns out to be in most applications, the flow is stable to small perturbations (ref.14). In the absence of mechanical vibrations, no secondary flow is possible at this level, the circumferential flow being stable and mostly of Couette type.

Outer region: centrifugal effects

The loss of contact between seal and shaft, combined with changes in the geometry, will introduce different features in the flow behavior as we go farther away from the gap. For a slowly-varying channel of height $d(z)$ on the outside (fig.1), we rescale the flow field by writing

$$(x,y,\xi) \to \left(\frac{z}{d}, \frac{r-R}{d}, \theta \right) \qquad , \qquad \tau \to \frac{\nu t}{d^2} \qquad (12)$$

$$(u,v,w) \to \left(\frac{d}{\nu} u_z, \frac{d}{\nu} u_r, \frac{u_\theta}{\Omega R} \right) \qquad , \qquad p^* \to \frac{(p-p_a)d^2}{\rho \nu^2} \qquad (13)$$

where d is some mean value of $d(z)$. It can be shown that the equations of motion, in the limit $\delta = d/R \to 0$, become

$$\nabla . \vec{u} = 0 \qquad (14)$$

$$(\partial_\tau + \vec{u}.\nabla) \vec{u} - T_a w^2 \hat{j} = -\nabla p^* + \nabla^2 \vec{u} \qquad (15)$$

$$(\partial_\tau + \vec{u}.\nabla) w = \nabla^2 w \qquad (16)$$

where

$$T_a = \frac{\Omega^2 R d^3}{\nu^2} \quad : \text{Taylor number} \qquad (17)$$

Note that the above system of equations are the so-called 'small-gap' equations, widely used in the context of the stability of axisymmetric Taylor-Couette flows (ref.15). Again, while the curvature effects are almost completely neglected, they are retained through the centrifugal term by imposing the Taylor number be held fixed as $\delta \to 0$. It follows that a rigid seal separated from a rotary shaft by a thin lubricating film is subject to centrifugal instabilities in a neighborhood of the contact area, driving eventually a secondary flow across the gap. Had we used these scales in the inner region

$$T_a = \frac{\Omega^2 R d^3}{\nu^2} \to \frac{\Omega^2 R h_o^3}{\nu^2} = \left(\frac{\Omega R h_o}{\nu} \right)^2 \frac{h_o}{R} = R_e^2 \, \delta \to 0 \quad \text{as } \delta \to 0 \qquad (18)$$

outer region | *inner region*

and the Taylor number indicates where curvature effects must be retained, regardless of the scales chosen.

In principle, the flow of lubricant fluid is governed by a set of equations similar to those of a stratified flow, where the centripetal acceleration plays the role of the buoyancy force, although for rotating flows whose inner surface moves the basic state could be unstable to small disturbances.

The domain under consideration is typically unbounded, and clearly some

502

difficulties arise with the introduction of artificial boundaries. It is known that isothermal flows with open boundaries can be successfully modeled employing the so-called natural boundary conditions, but other techniques are needed to solve the more complicated problem of buoyancy-driven flows, where the use of the natural boundary conditions is precluded by the additional pressure gradient generated by the buoyancy term (refs. 16 to 18).

In the next section we address the appropriate use of the penalty formulation in the finite element method for unbounded flows in presence of variable body forces. Finally, we will see how different open boundary conditions can lead to contradictory predictions in the flow behavior.

PENALTY FUNCTION FORMULATION FOR THE N-S EQUATIONS

In what follows, we denote the coordinate directions as (x, y) or (x_1, x_2), the transverse velocity components as (u, v) or (u_1, u_2), the azimuthal component of the velocity as w, and the pressure as p; δ_{ij} is the Kronecker delta. For convenience in the treatment of the boundary conditions, we rewrite the equations of motion as

$$\frac{\partial u_i}{\partial x_i} = 0 \tag{19}$$

$$\frac{\partial u_i}{\partial t} + u_j \frac{\partial u_i}{\partial x_j} = T_a \, w^2 \, \delta_{i2} + \frac{\partial \sigma_{ij}}{\partial x_j} \tag{20}$$

$$\frac{\partial w}{\partial t} + u_j \frac{\partial w}{\partial x_j} = \frac{\partial^2 w}{\partial x_j \partial x_j} \tag{21}$$

The Taylor number T_a is defined in equation (17), and the stress in the fluid is given now by

$$\sigma_{ij} = - p \delta_{ij} + \left(\frac{\partial u_i}{\partial x_j} + \frac{\partial u_j}{\partial x_i} \right) \tag{22}$$

A weak form is obtained by taking the inner product of the transverse momentum equations (20) with a weighting function $\vec{W} = (W_1, W_2)$, and multiplying the azimuthal momentum equation (21) by a scalar function W. The penalty method is implemented by introducing the pseudo-constitutive relation (ref.19)

$$p = p_s - \lambda \frac{\partial u_j}{\partial x_j} \tag{23}$$

where p_s is the hydrostatic pressure for a fluid at rest and λ is the penalty parameter. Upon application of Green's theorem and substituting p by the above expression, we get

$$\int_\Omega \left(\frac{\partial u_i}{\partial t} + u_j \frac{\partial u_i}{\partial x_j} \right) W_i \, d\Omega + \lambda \int_\Omega \frac{\partial u_j}{\partial x_j} \frac{\partial W_i}{\partial x_i} \, d\Omega + \int_\Omega \left(\frac{\partial u_i}{\partial x_j} + \frac{\partial u_j}{\partial x_i} \right) \frac{\partial W_i}{\partial x_j} \, d\Omega = V_f + S_f \tag{24}$$

$$\int_\Omega \left(\frac{\partial w}{\partial t} + u_j \frac{\partial w}{\partial x_j} \right) d\Omega + \int_\Omega \frac{\partial w}{\partial x_j} \frac{\partial W}{\partial x_j} \, d\Omega = \int_{\partial \Omega} W \frac{\partial w}{\partial x_j} n_j \, ds \tag{25}$$

where the surface forces S_f and the volume forces V_f are defined by

$$S_f = \int_{\partial \Omega} [- p \, W_i \, n_i + W_i \left(\frac{\partial u_i}{\partial x_j} + \frac{\partial u_j}{\partial x_i} \right) n_j] \, ds \tag{26}$$

$$V_f = \int_\Omega T_a \, w^2 \, \delta_{i2} \, W_i \, d\Omega \tag{27}$$

and $\hat{n} = (n_1, n_2)$ is the unit vector normal to the boundary $\partial\Omega$ and pointing outwards. On a vertical boundary with normal $\hat{n} = (1,0)$, the integrand of S_f reduces to

$$\vec{W} = (W_1, 0): \quad -p + 2\frac{\partial u}{\partial x} \tag{28}$$

for normal traction, and

$$\vec{W} = (0, W_2): \quad \frac{\partial u}{\partial y} + \frac{\partial v}{\partial x} \tag{29}$$

for shear traction, in a weak rather than a pointwise sense.

Boundary conditions

The boundary conditions are the usual no-slip and no mass penetration at solid walls on the physical boundaries. This is, $u = v = 0$ and $w = 1$ at the lower boundary $y = 0$, which represents the outer surface of the rotating shaft, and $u = v = w = 0$ at the upper boundary, which is stationary.

At the open boundaries, on both sides of the contact region, the following two open boundary conditions (OBC) are employed for the flow field.

(i) Stress-free or natural boundary condition (NBC). We set the normal and shear stresses in equation (26) equal to zero.

(ii) Free-boundary condition (FBC). We evaluate the line integrals (26) of the weak form of the momentum equations using values computed on the outflow elements. Then, we force the line integrals into the right-hand-side of the discretized equations until convergence is achieved (refs. 17 and 18).

The natural boundary condition $\partial w/\partial n = 0$ is used in the weak form of the transport equation (25) instead.

FINITE ELEMENT METHOD

We discretize the domain into M elements and N nodes, and we expand the velocity components using bilinear quadrilateral elements and piecewise constant elements for pressure. All terms of the weak form of the governing equations are evaluated with full Gaussian quadrature, except the penalty term, where selective reduced integration is used (ref.20). The weighting functions are set equal to the basis functions, except in the convective terms, where perturbed Petrov-Galerkin functions with balancing tensor diffusivity are employed (refs.21 and 22). The time integration is based on the theta method with lumped mass matrices in the time derivatives. The numerical evaluation of the weighted residuals of the momentum equations leads to a nonlinear system of equations that is solved by Newton iteration using a direct solver based on Gauss elimination for unsymmetric banded matrices (ref.23). A convergence tolerance less than 1% of the relative change $\| \Delta u^\nu \| / \| u^\nu \|$ in the velocity field is imposed to terminate each full ν-th Newton iteration. The pressure p_e over each element Ω_e is calculated using the weak form of the relation (23)

$$p_e = -\frac{\lambda}{\Omega_e} \int_{\Omega_e} \nabla \cdot \vec{u} \, d\Omega \tag{30}$$

504

where the cross bar denotes selective reduced integration.

To march in time we use the velocity field u^n and pressure p^n at time t_n to evaluate the terms of S_f and V_f of the buoyancy force vector b^n. Having determined b^n, we compute the velocity field using the Newton linearization algorithm. Once u^{n+1} is known, we update the pressure by means of the equation (30) and solve the transport equation for w^{n+1}. The scheme is repeated until steady state is achieved. Time integration is terminated when the relative change between time steps is

$$\left\| \frac{u^{n+1} - u^n}{u^{n+1}} \right\| < \epsilon_1 \quad \text{and} \quad \left\| \frac{w^{n+1} - w^n}{w^{n+1}} \right\| < \epsilon_2 \qquad (31)$$

where

$$\| u \| = \sum_{j=1}^{2N} | u_j |$$

for some prescribed error tolerances ϵ_1 and ϵ_2. All the following results are obtained with the fully implicit algorithm starting from zero initial conditions.

NUMERICAL EXAMPLES

Preliminary computations showed the necessity of using mesh grading as the contact region is approached from both sides. Transition elements are also employed to avoid extremely small elements in the contact area.

The geometry and the finite element mesh employed for the present calculations are shown in fig. 2. Details of the discretization can be appreciated in fig.3. The mesh contains 2035 nodes and 1864 elements, and the penalty parameter λ is equal to 10^8 in all cases. The relevant lengths are $b = 200\mu m$, which is used as reference length, $h_o = 10\mu m$, and $R = 0.035m$.

The pressure is adjusted at every time step in such a way that is always zero at the first element (located at $x = -11$, $y = 0$), and the line integrals (26) are evaluated, if the OBC requires so, with values computed on the outflow elements.

Results of the transverse velocity field, the azimuthal component of the velocity, and the pressure obtained with the FBC at the open boundaries are all shown in fig.4, and continues up to fig.7. The simulation corresponds to a Taylor number $T_a = 15$. The steep pressure gradient developed across the gap is shown in fig.5, and the resultant flux of lubricant flowing from the air-side to the oil-side is observed in fig.6. Streamline contours are plotted in fig.7. Similar results obtained with the NBC at the outlets can be seen from fig.8 to fig.11. The striking differences in the numerical predictions of both OBC are better illustrated in fig.7 and fig.11. The former clearly shows that an improper treatment of the open boundary conditions causes backflow into the computational domain. The intensity of the returning flow due to the NBC at the air-side outflow boundary induces a cell structure in an otherwise almost plane Couette flow (see w in fig.4).

CONCLUSIONS

The geometry and, in particular, the tiny size of the gap imposes a severe constraint in the numerical simulation. Furthermore, we have seen that an improper specification of the outflow boundary condition can cause artificial returning flow which, for the present problem, spoils the solution in the whole computational domain. Both boundary conditions show that centrifugal instabilities play an important role in the
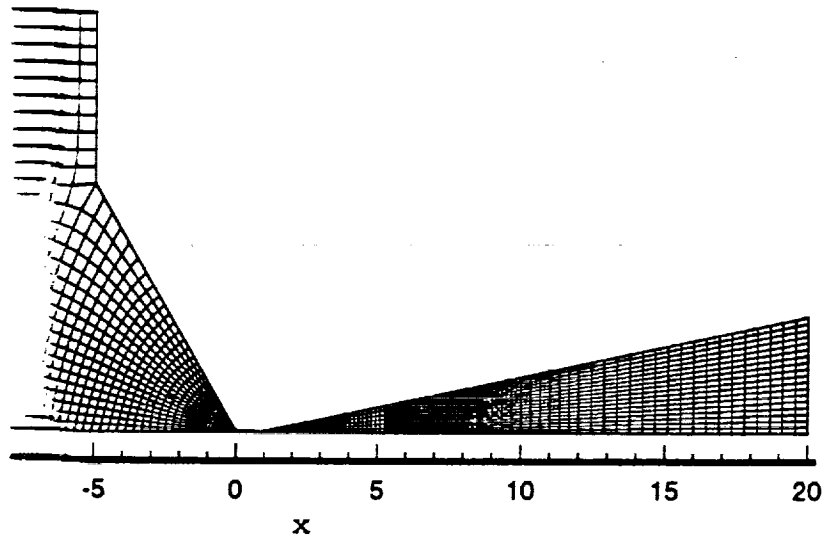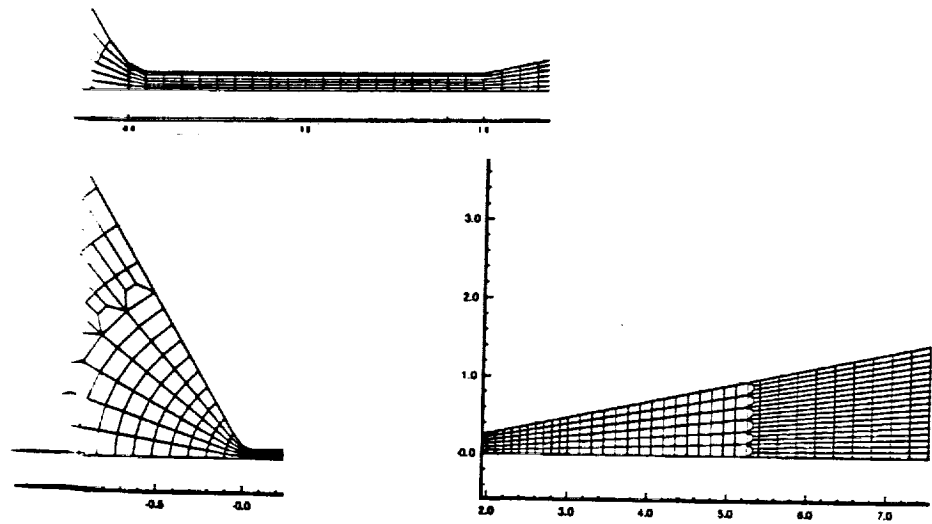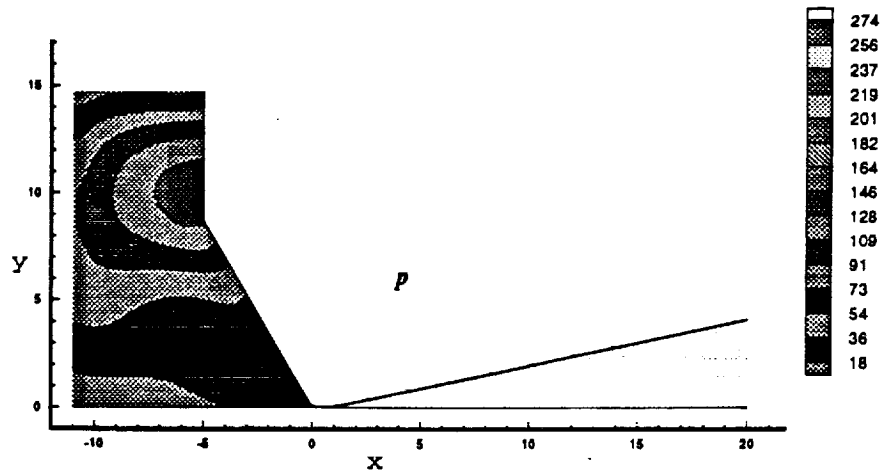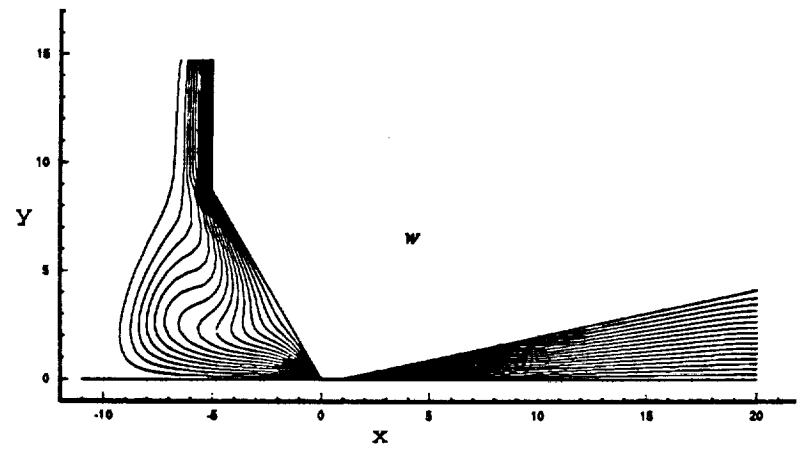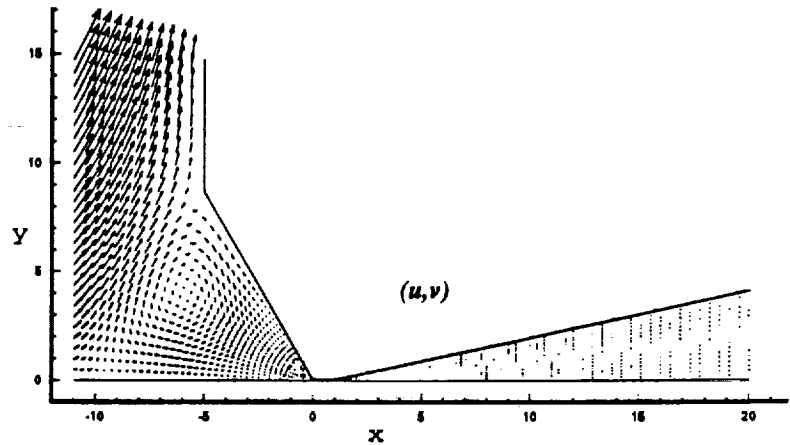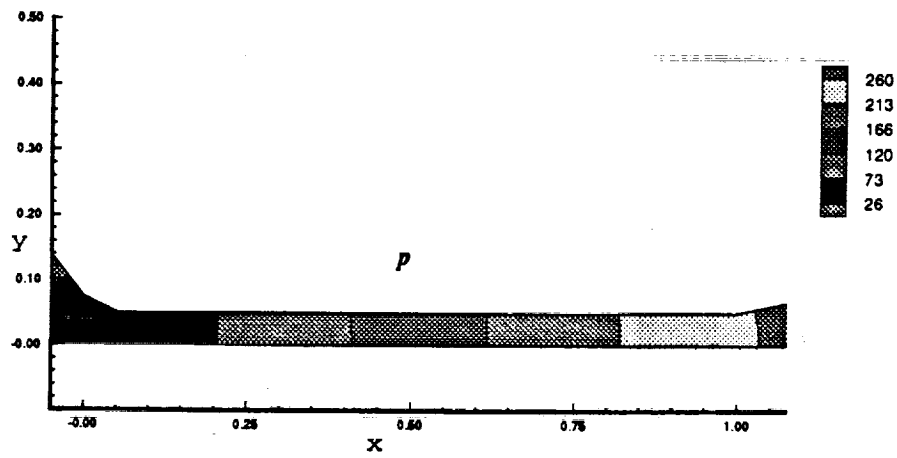
figure 2

figure 3

figure 4

figure 5
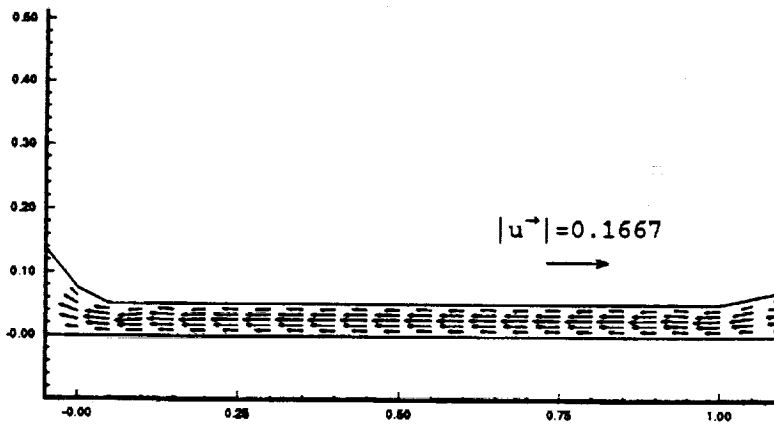
figure 6
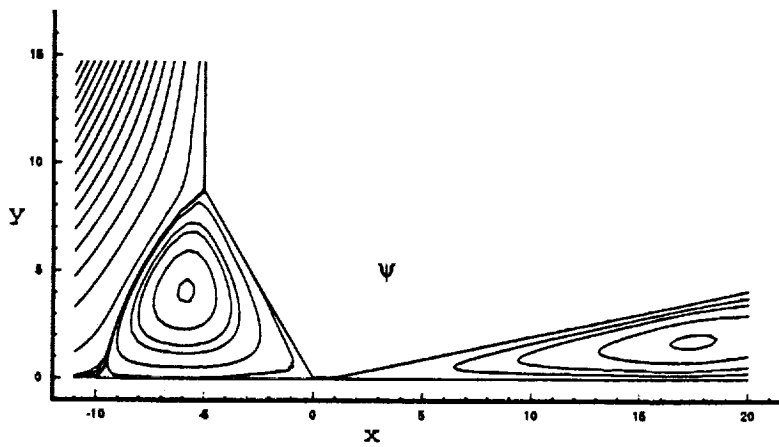
figure 7
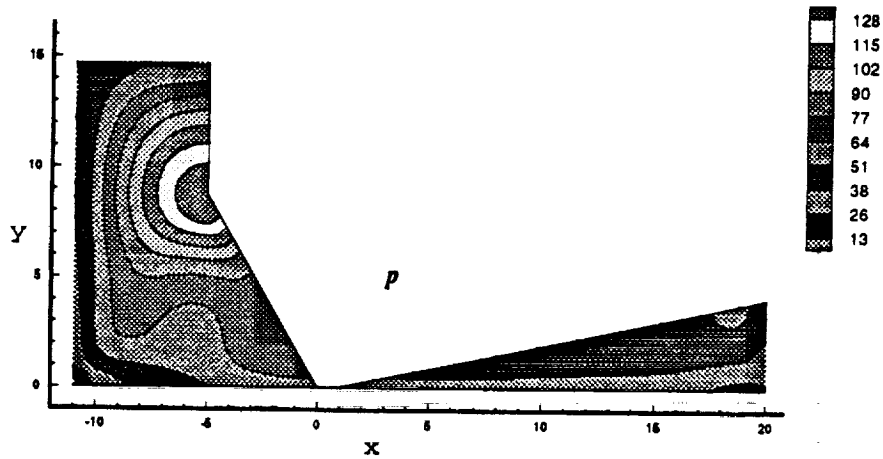
figure 8

figure 9
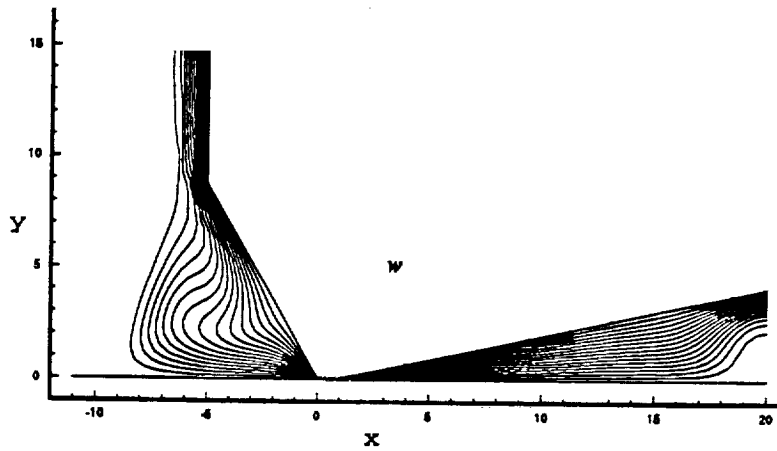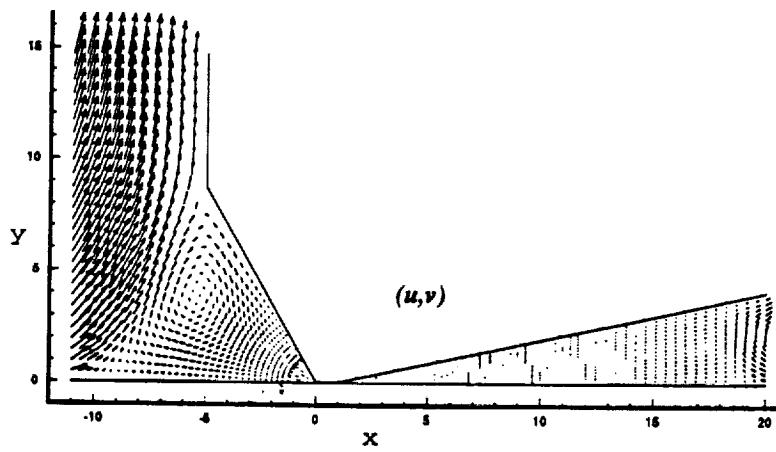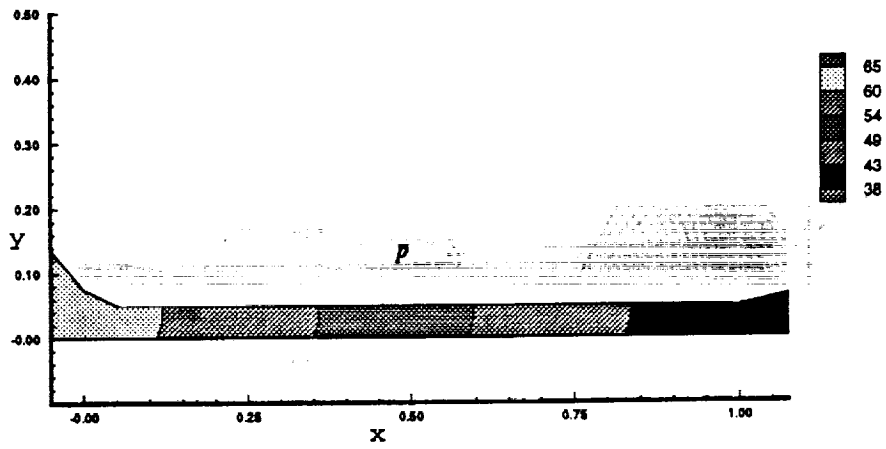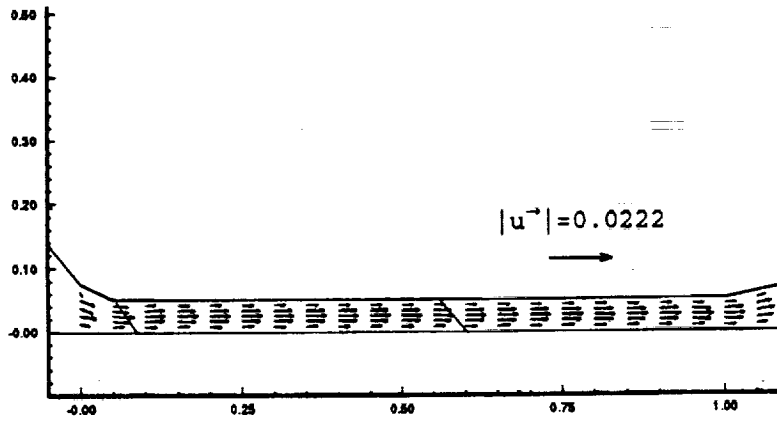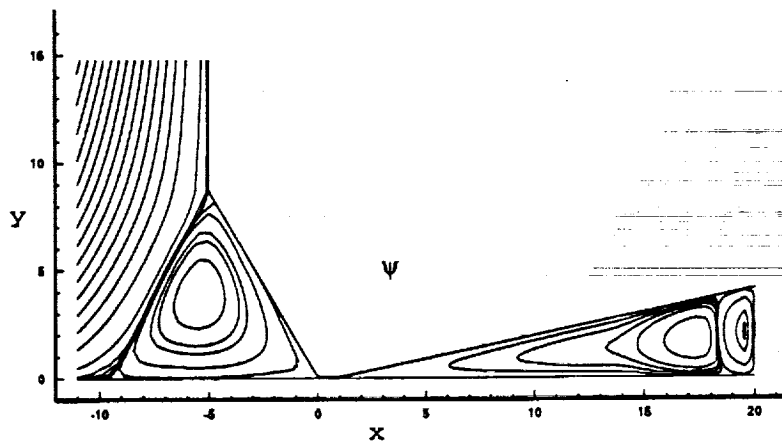

figure 10

figure 11

sealing mechanisms of the type of devices here studied, even when their predictions are contradictory. While the NBC suggests leakage, the FBC indicates that sealing is achieved by pumping oil from the air-side, where the azimuthal flow is stable, to the oil-side, where centrifugal instabilities set in.

It is known that the use of the NBC in presence of variable body forces leads to erroneous results (refs.16 and 18). On the contrary, the application of the FBC is equivalent to a radiating boundary able to filter unwelcome reflections towards the interior of the computational domain (ref.24).

Besides its simplicity, the capability of the small-gap limit in incorporating the physics of the flow of lubricant fluid through the micro-gap of sealing devices has been established. Other effects, such as capillary forces on the oil-air interface and temperature variations should be included in future works.

REFERENCES

1. Jagger, E.T.: Study of the Lubrication of Synthetic Rubber Rotary Shaft Seals. Proc. Conf. on Lubrication and Wear. Inst. of Mech. Eng., 1957, pp.409-415.
2. Kawahara, Y.; and Hirabayashi, H.: A Study of Sealing Phenomena on Oil Seals. ASLE 77-LL-5B-2, 1977.
3. Hirano, F.; Ishiwata, H.; and Kambayashi, H.: Frictional Sealing Characteristics of Oil Seals. Proc. 1st. Int. Conf. on Fluid Sealing, BHRA, 1961, pp. 698-709.
4. Davies, M.G.: The Generation of Lift by Surfaces Roughness in Radial Face Seals. Int. Conf. on Fluid Sealing. B.H.R.A., 1961, Cranfield, England.
5. Jagger, E.T.; and Walker, P.S.: Further Studies of the Lubrication of Synthetic Rubber Shaft Seals. Proc. Inst. Mech. Engrs. Vol.181, 1966-1967, pp. 101-204.
6. Lebeck A.O.: Parallel Sliding Load Support in the Mixed Friction Regime. Part 1. The Experimental Data. *ASME Journal of Tribology*, 1986, Vol. 109.
7. Lebeck A.O.: Parallel Sliding Load Support in the Mixed Friction Regime. Part 2. Evaluation of the Mechanisms. *ASME Journal of Tribology*, 1986, Vol. 109.
8. Gabelli A.; and Poll, G.: Formation of Lubricant Film in Rotary Sealing Contacts: Part I - Lubricant Film Modeling. Paper No.90-Trib-64, ASME/STLE Tribology Conference, 1990, Toronto, Canada.
9. Salant R.F.: Numerical Analysis of the Flow Field within Lip Seals Containing Microundulations. Paper No.91-Trib-45, STLE/ASME Tribology Conference, 1990, St. Louis, Mo.
10. Gabelli A.: Private communication, 1992.
11. Johnston D.E.: Theoretical Analysis of a Pumping Mechanism Between Relatively Moving Surfaces. Proc. BHRA 12th. Int. Conf. Fluid Sealing. 1989, Brighton, UK.
12. Batchelor G.K.: An Introduction to Fluid Dynamics. Cambridge University Press, 1967.
13. Krueger E.R.; Gross, A.; and Di Prima, R.C.: On the Relative Importance of Taylor-vortex and Non-axisymmetric Modes in Flow Between Rotating Cylinders. *J. Fluid Mech.*, Vol.24, part 3, 1966, pp.521-538.
14. Drazin P.G.; and Reid, W.H.: Hydrodynamic Stability. Cambridge University Press, 1981.
15. Hall P.: The Stability of Unsteady Cylinder Flows. *J. Fluid Mech.*, Vol.67, part 1, 1975, pp.29-63.
16. Leone J. M.: Open Boundary Condition Symposium. Benchmark Solution: Stratified Flow over a Backward-facing Step. *Int. J. Num. Meth. in Fluids* Vol.11, 1990, pp 969-984.
17. Papanastasiou T.C.; Malamataris N.; and Ellwood, K.: A New Outflow Boundary

Condition. *Int. J. Num. Meth. Fluids*, Vol.14, 1992, pp.587-608.

18. Vionnet, C.A.; and Heinrich, J.C.: Open Boundary Conditions for Viscous Flows with Variable Body Forces. To be presented at the ASME WAM 93, Advances in Finite Element Analysis in Fluid Dynamics III. Nov. 1993, New Orleans, Louisiana.

19. Heinrich, J.C.; and Marshall, R.S.: Viscous Incompressible Flow by a Penalty Function Finite Element Method. *Computer and Fluids*, Vol.9, 1981, pp 73-83.

20. Carey G.F.; and Oden, J.T.: Finite Elements. Fluid Mechanics. Vol. VI, 1986, Prentice-Hall, Inc.

21. Brooks A.N.; and Hughes, T.J.R.: Streamline Upwind/Petrov Galerkin Formulations for Convection Dominated Flows with Particular Emphasis on the Incompressible Navier-Stokes Equations. *Comp. Meth. in Appl. Mech. and Eng.*, Vol.32, 1982, pp.199-259.

22. Heinrich, J.C.; and Yu, C.C.: Finite Element Simulation of Buoyancy-Driven Flows with Emphasis on Natural Convection in a Horizontal Circular Cylinder. *Comp. Meth. Appl. Mech. Eng.*, Vol.69, 1988, pp.1-27.

23. Dongarra, J.J.; Bunch, J.R.; Moler, C.B.; and Stewart, G.W.: LINPACK User's Guide, SIAM, 1979, Philadelphia.

24. Heinrich, J.C.; and Vionnet, C.A.: On Boundary Conditions for Unbounded Flows. Submitted for publication to *Communications in Applied Numerical Methods*. Wiley and Sons.